Scientific Research Publishing

Open Journal of Biophysics, 2023, 13, 35-49
https://www.scirp.org/journal/ojbiphy
ISSN Online: 2164-5396
ISSN Print: 2164-5388

In Silico Evaluation of the Potential Interference of Boceprevir, Calpain Inhibitor II, Calpain Inhibitor XII, and GC376 in the Binding of SARS-CoV-2 Spike Protein to Human Nanobody Nb20

Yuri Alves de Oliveira Só[1*], Marcelo Lopes Pereira Junior[2], Wiliam Ferreira Giozza[2], Rafael Timóteo de Sousa Junior[2], Ricardo Gargano[1], Luiz Antônio Ribeiro Júnior[1]

[1]Institute of Physics, University of Brasília, Brasília, Brazil
[2]Department of Electrical Engineering, University of Brasília, Brasília, Brazil
Email: *yurialves.y@gmail.com

How to cite this paper: de Oliveira Só, Y.A., Junior, M.L.P., Giozza, W.F., de Sousa Junior, R.T., Gargano, R. and Júnior, L.A.R. (2023) In Silico Evaluation of the Potential Interference of Boceprevir, Calpain Inhibitor II, Calpain Inhibitor XII, and GC376 in the Binding of SARS-CoV-2 Spike Protein to Human Nanobody Nb20. *Open Journal of Biophysics*, **13**, 35-49.
https://doi.org/10.4236/ojbiphy.2023.133004

Received: July 3, 2023
Accepted: July 25, 2023
Published: July 28, 2023

Abstract

Virtual screening can be a helpful approach to propose treatments for COVID-19 by developing inhibitors for blocking the attachment of the virus to human cells. This study uses molecular docking, recovery time and dynamics to analyze if potential inhibitors of main protease (M^{pro}) of SARS-CoV-2 can interfere in the attachment of nanobodies, specifically Nb20, in the receptor binding domain (RBD) of SARS-CoV-2. The potential inhibitors are four compounds previously identified in a fluorescence resonance energy transfer (FRET)-based enzymatic assay for the SARS-CoV-2 M^{pro}: Boceprevir, Calpain Inhibitor II, Calpain Inhibitor XII, and GC376. The findings reveal that Boceprevir has the higher affinity with the RBD/Nb20 complex, followed by Calpain Inhibitor XII, GC376 and Calpain Inhibitor II. The recovery time indicates that the RBD/Nb20 complex needs a relatively short time to return to what it was before the presence of the ligands. For the RMSD the Boceprevir and Calpain Inhibitor II have the shortest interaction times, while Calpain Inhibitor XII shows slightly more interaction, but with significant pose fluctuations. On the other hand, GC376 remains stably bound for a longer duration compared to the other compounds, suggesting that they can potentially interfere with the neutralization process of Nb20.

Keywords

SARS-CoV-2, Main protease M^{pro}, Boceprevir, Calpain Inhibitor II, Calpain

Inhibitor XII, GC376, Nanobody Nb20, In Silico

1. Introduction

Global efforts have focused on developing vaccines and antiviral drugs to combat the COVID-19 disease caused by the SARS-CoV-2 coronavirus, which reached the pandemic in March 2020 [1]-[6]. As of June 2023, the virus has infected over 767 million individuals and caused over 6.9 million deaths worldwide [7] [8]. Recent successes have resulted in the production of vaccines being administered [9] [10] [11] [12]. However, despite the initiation of vaccination programs, no effective treatment for individuals already infected with the virus has been universally agreed upon.

Nanobodies, which are small antibodies found in camelids like llamas and camels, possess unique characteristics that make them highly effective in binding to specific antigens, including proteins of the SARS-CoV-2 virus [6] [13] [14]. These nanobodies have garnered considerable attention as a promising therapeutic approach against COVID-19. They can be engineered to target various virus proteins, such as the spike protein found in the receptor binding domain (RBD), the main protease, and other viral proteins. By doing so, they inhibit the function of these proteins and hinder viral entry into host cells and replication [15] [16].

Compared to traditional antibodies, nanobodies offer several potential advantages. They have a compact size, which facilitates large-scale production and enhances stability. Moreover, they can be precisely designed to bind to specific regions of viral proteins, reducing the risk of mutations that could undermine the treatment's effectiveness [17] [18].

At the same time, numerous drugs have been extensively studied and proposed to combat SARS-CoV-2, employing diverse mechanisms, whether acting on the RBD of SARS-CoV-2 or on the main protease (M^{pro}) that participates in the viral replication process [19] [20] [21] [22]. These drugs can potentially interfere with the function of nanobodies or work synergistically to enhance treatment outcomes. Given these features, we selected four compounds: Boceprevir, Calpain Inhibitor II, Calpain Inhibitor XII, and GC376. These compounds were previously identified in a fluorescence resonance energy transfer (FRET)-based enzymatic assay targeting the SARS-CoV-2 the M^{pro} [23] [24]. They have demonstrated potent activity, with IC_{50} values ranging from single-digit to submicromolar concentrations in the enzymatic assay [23].

In this study, we conducted molecular docking and dynamics analyses to investigate the potential interactions of the four previously mentioned compounds, which are known to interact with M^{pro}. We aimed to estimate whether these compounds could interfere with the neutralization process of RBD of SARS-CoV-2 by the human nanobody Nb20 or potentially act synergistically to improve the treat-

ment against SARS-CoV-2.

2. Materials and Methods

2.1. Protein Preparation

Figure 1 presents the critical proteins involved in the RBD/Nb20 interaction obtained from Protein Data Bank, ID 7JVB [17]. In Figure 1(a), the Nb20 protein is blue, while the Sars-CoV-2 RBD is red. We highlighted the inhibition region between these proteins with a black square in Figure 1(b). The GLN493, ARG31, TYR104, GLU484, and ARG97 are the residues that interact via hydrogen bonds within the RBD/Nb20 interface. Table 1 shows the residues participating in the Nb20/SARS-Cov-2 interactions and respective distances for the hydrogen bonds. Figure 1(c) illustrates the binding site surface using the following color code: grey, red, blue, and white for carbon, oxygen, nitrogen, and hydrogen atoms, respectively. The protein resolution is 2.45 Å, and no pKa prediction was performed. We have considered all the crucial residues in the RDB/Nb20 interface and only metal ions in the docking study.

2.2. Ligand Preparation

The Boceprevir, Calpain Inhibitor II, Calpain Inhibitor XII, and GC376 3D structures were extracted from PubChem [25]. The chemical structures of these compounds are presented in Figure 2, while relevant information such as PubChem ID, molecular weight, and molecular formula is shown in Table 2.

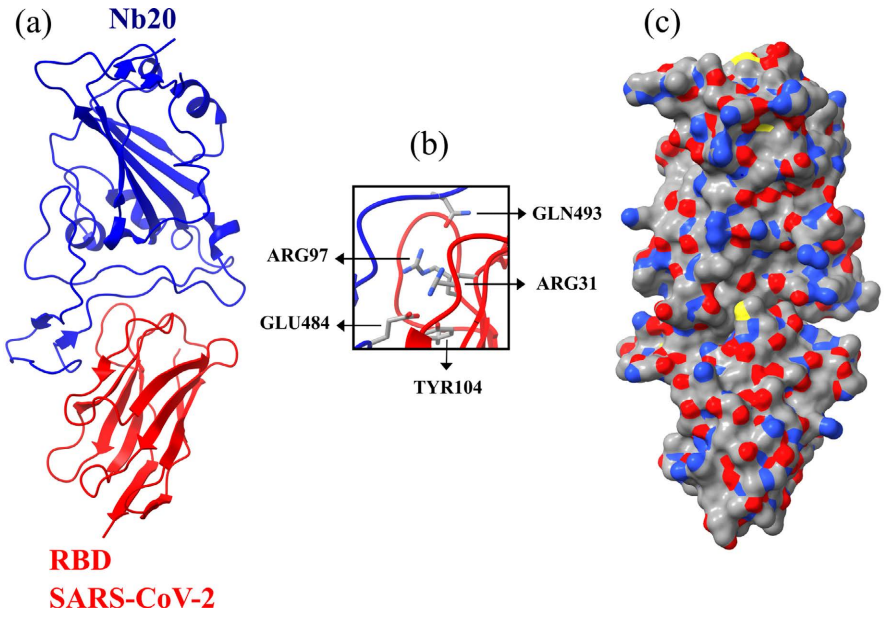

Figure 1. Schematic representation of the (a) main proteins involved in RBD/Nb20 interaction. These proteins were obtained from Protein Data Bank, ID 7JVB. (b) The GLN493, ARG31, TYR104, GLU484, and ARG97 are the residues that interact via hydrogen bonds within the RBD/Nb20 interface. (c) The binding site surface has the following color scheme: grey, red, blue, and white for carbon, oxygen, nitrogen, and hydrogen atoms, respectively.

Table 1. Residues participating in the nanobody Nb20/SARS-CoV-2 interactions and respective distances for the hydrogen bonds.

Hydrogen Bonds				
Nanobody Nb20		SARS-CoV-2		2*Distance H-A (Å)
Aminoacid	Residue	Aminoacid	Residue	
GLN	493	SER	494	3.586
GLN	493	ALA	29	2.939
GLN	493	ARG	97	3.133
LEU	492	ARG	97	3.372
PHE	490	ARG	97	3.267
GLU	484	TYR	104	2.267
GLU	484	ARG	31	3.085
GLU	484	ARG	31	2.562
GLU	484	ARG	31	3.167
MET	55	ARG	31	2.838
MET	55	ARG	31	2.676

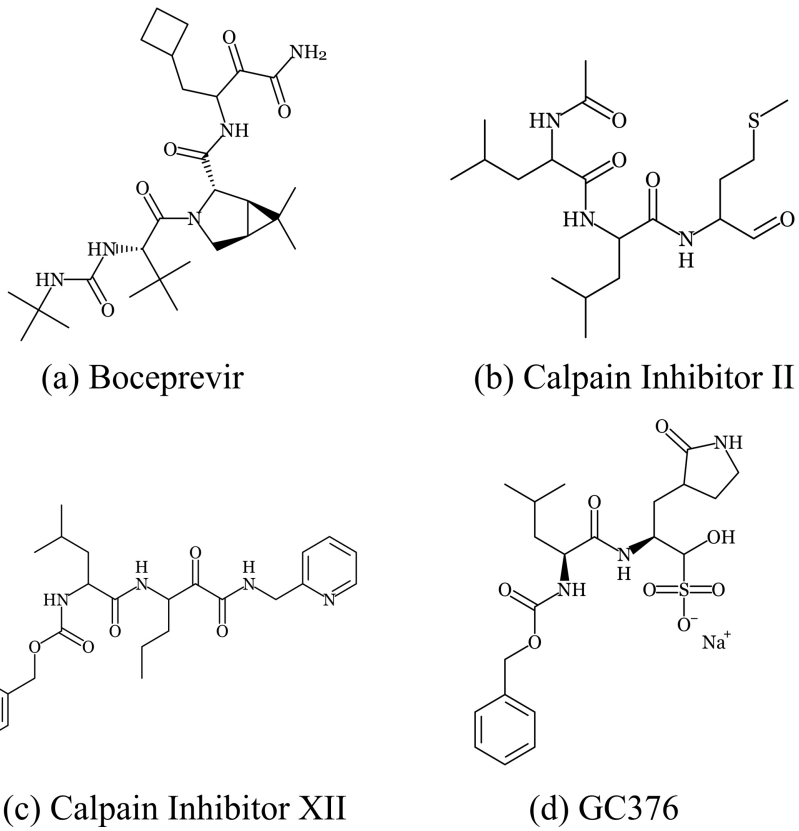

Figure 2. Schematic representation of the chemical structure of (a) Boceprevir, (b) Calpain Inhibitor II, (c) Calpain Inhibitor XII, and (d) GC376.

Table 2. Extra information of Boceprevir, Calpain Inhibitor II, Calpain Inhibitor XII, and GC376.

Compound	PubChem CID	Molecular Weight [g/mol]	Molecular Formula
Boceprevir	10,324,367	519.7	$C_{27}H_{45}N_5O_5$
Calpain Inhibitor II	20,086,354	378.5	$C_{20}H_{30}N_2O_5$
Calpain Inhibitor XII	16,760,340	482.6	$C_{26}H_{34}N_4O_5$
GC376	71,481,119	507.5	$C_{21}H_{30}N_3NaO_8S$

2.3. Molecular Docking Simulations

We used molecular docking simulations to analyze the non-covalent binding between the RBD/Nb20 protein complex (see **Figure 1**) and four small molecules presented in **Figure 2**. The docking simulations were conducted using the Webina-autodock 1.0.2 server [26], which employs the Chemistry at HARvard Macromolecular Mechanics (CHARMM) force field and a blind docking strategy [27].

The Protein-Ligand Interaction Profiler (PLIP) server [28] was used to characterize the interaction between each compound and the RBD/Nb20 complex, with a focus on the interface between the two proteins, which is crucial for blocking coronavirus entry and replication, see **Figure 1(b)**. The simulation box used for ligand screening was also limited to this interface, with dimensions of 28 Å × 0 Å × 10 Å, and a center point of (32, −36, 2) Å, which corresponds to the region of primary interest, consisting of the main interaction site between the RBD of SARS-CoV-2 and Nb20 protein. The ligand positions and binding affinities were estimated with an accuracy of ±2 Å, and ±0.01 Kcal/mol, respectively.

2.4. Recovering Time Calculations

The recovery time (τ) [29] [30] of a substance after it has adsorbed on a solid surface can be calculated using the following equation from transition state theory:

$$\tau = \nu_0^{-1} \mathrm{e}^{E_{ad}/k_B T}, \tag{1}$$

were, ν_0 is the attempt frequency, which is approximately 10^{12} s^{-1} [31], T is the temperature (set to 300 K), k_B is Boltzmann's constant, and E_{ad} is the desorption energy. Desorption refers to releasing a substance from the interface between a solid surface and a solution. According to the equation above, a more negative value of E_{ad} leads to a longer recovery time. In other words, the activation energy (E_a) required to overcome the desorption process is directly proportional to E_{ad}. Thus, the recovery time can be used to estimate the time required for a complex to return to what it was before the presence of the ligand.

2.5. Molecular Dynamics Simulations

Additionally, we performed a molecular dynamics (MD) simulation with a time

on the order of the smallest value obtained for the recovery time, using the NAMD computational package [32] and CHARMM36 [33] force field, to estimate if the ligands can quickly escape the chosen binding site and, thus, not interfere with the RBD/Nb20 interactions. If the ligands are not stable in the region of RBD/Nb20 interaction, they are expected to not compete with Nb20. The number of molecules, pressure, and temperature were kept constant using Langevin dynamics in the NPT ensemble at 300 K and 1 atm, respectively. We computed the system's temporal evolution to calculate the Root Mean Square Deviation (RMSD). The MD snapshots, trajectories, and RMSD calculations were obtained using the visualization and analysis software (VMD) [34].

3. Results and Discussion

We begin our discussion by presenting the molecular docking results. The ligand poses with the lowest binding energy affinity (ΔG free energy) were selected based on their docking scores, corresponding to the most likely and stable binding modes [35].

The results of the docking simulations are presented in **Table 3**, and they indicate that all four ligands have significant binding affinities for the target proteins. Among them, Boceprevir shows the highest binding affinity for the RBD/Nb20 proteins, with a value of approximately −7.3 Kcal/mol, while Calpain02 exhibited the lowest binding affinity of about −5.4 Kcal/mol. We observed that the ligands with a higher molecular weight tended to have more stable docking results, evident when contrasting information in **Table 2** and **Table 3**.

In previous studies, similar binding affinity results for other ligand species were reported for the interaction of RBD with the human angiotensin-converting enzyme 2 (ACE-2) protein, with docking scores ranging from −3.2 to −9.8 kcal/mol [36] [37]. In **Table 3**, the docking affinities of the ligands are comparable to the ones for (S,S)-2-1-carboxy-2-[3-(3,5-dichlorobenzyl)-3H-imidazol4-yl]-ethylamino-4-methylpentanoic acid (MLN-4760). This potent inhibitor alters the conformation of ACE-2 and prevents the binding of SARS-CoV-2 and ACE-2 [38]. The docking score of MLN-4760 was −7.28 kcal/mol, similar to Boceprevir's docking score in this study.

Table 3. Lowest binding affinities ΔG (in Kcal/mol) obtained for the ligands studied here, when interacting with RBD/Nb20 proteins.

Compound	ΔG [Kcal/mol]
Boceprevir	−7.3
Calpain Inhibitor II	−5.4
Calpain Inhibitor XII	−6.2
GC376	−6.0

In Figure 3, the binding site surfaces (BSS) are presented for the ligand conformations with the RBD/Nb20 proteins, showing the best results in molecular docking simulations. Only the region of interest displayed in Figure 1(b) is depicted. The color code used to represent the different atoms is grey, red, blue, and white, indicating carbon, oxygen, nitrogen, and hydrogen, respectively. The ball-and-stick representation uses cyan, red, and white to show carbon, oxygen, and hydrogen atoms. Overall, the ligands fit nicely inside the cavity, which is the core pocket region of the RBD/Nb20 proteins, shown in Figure 1(a). Boceprevir, Calpain Inhibitor II, Calpain Inhibitor XII, and GC376 exhibited adsorption regions in the interaction with the RBD/Nb20 complex and tended to interact with oxygen and nitrogen atoms.

The interactions between amino acid residues of RBD/Nb20 proteins and ligands are depicted in Figure 4, generated using PLIP. The ligands are represented as sticks, with carbon and oxygen atoms in orange and red, respectively. The color code highlights hydrophobic interactions in red, hydrogen bonds in green, π-stacking in blue, and salt bridges in purple. Figure 4 illustrates that Boceprevir (Figure 4(a)), Calpain Inhibitor II (Figure 4(b)), Calpain Inhibitor XII (Figure 4(c)), and GC376 (Figure 4(d)) interact with RBD/Nb20 proteins mainly through 2, 4, 1, and 3 hydrogen bonds and 6, 3, 5, and 3 hydrophobic interactions with distinct amino acid residues in both RBD and Nb20 proteins. Additionally, Figure 4(c) shows an π-stacking interaction between RBD/Nb20 and Calpain Inhibitor XII, while a salt bridge interaction with GC376 is visible in Figure 4(d).

Table 4 presents all the interactions between amino acid residues of RBD/Nb20 proteins and the ligands, along with their respective distances. Thirteen amino acid residues of the RBD/Nb20 proteins were identified as interacting with the ligands. Specifically, the RBD amino acid residues involved were ILE294 (5), ALA224 (1), GLU295 (2), SER162 (1), and HIS225 (1), while the

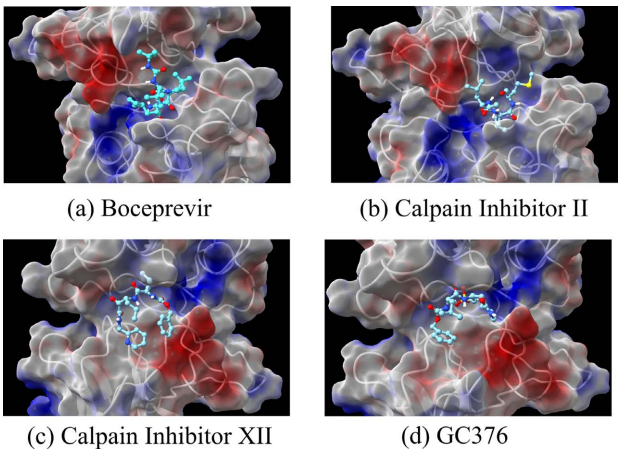

Figure 3. Schematic representation of the binding site surface (BSS) for the presumed best docking target/ligand configurations of (a) Boceprevir, (b) Calpain Inhibitor II, (c) Calpain Inhibitor XII, and (d) GC376.

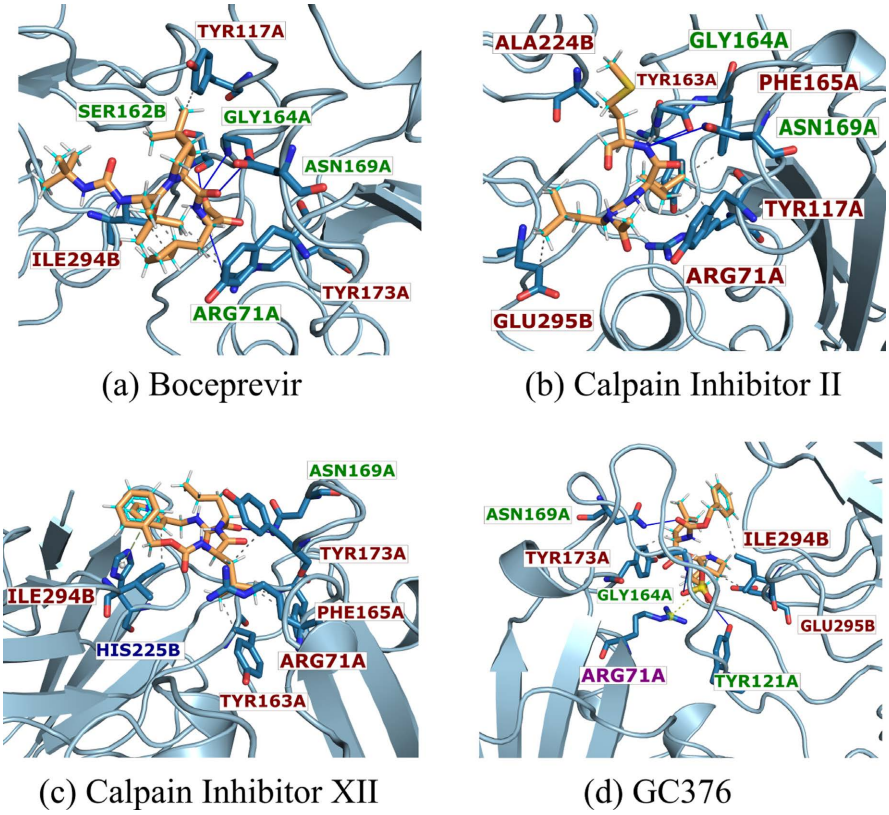

Figure 4. PLIP docked poses for the RBD/Nb20 interaction with (a) Boceprevir, (b) Calpain Inhibitor II, (c) Calpain Inhibitor XII, and (d) GC376. The index A at the end of the amino acid name represents that it belongs Human Nanobody Nb20 receptor and B the SARS-CoV-2. The font color in red represents hydrophobic interactions, green hydrogen bonds, blue π-stacking, and purple salt bridges.

Nb20 amino acid residues were TYR117 (1), TYR173 (5), TYR163 (2), TYR121 (2), ARG71 (4), PHE165 (2), GLY164 (3), and ASN169 (4). Based on their higher occurrence, the results suggest that the target amino acid residues for this set of ligands are ARG71 and ASN169 from Nb20 and ILE294 from RBD.

Notably, Calpain Inhibitor II and Calpain Inhibitor XII exhibit higher hydrophobic interactions, while Boceprevir shows higher hydrogen bonds, and GC376 has quantities of hydrophobic interactions and hydrogen bonds equal. Additionally, the number of times the amino acid with the highest interaction (TYR) interacts with the ligands can be estimated, corresponding to ten interactions (eight hydrogen bonds and two hydrophobic interactions). This finding suggests that TYR is a significant amino acid in promoting attachment to RBD for this set of ligands (see Figure 5).

Based on the docking results, we calculate the recovery time (Equation (1)) of the proteins/ligand complexes to estimate if the ligands (Boceprevir, Calpain Inhibitor II, Calpain Inhibitor XII, and GC376) interacted with the complex RBD/Nb20 for a short or long time. The recovery time represents the time necessary for the proteins to return to their original conformation. Table 5 presents the complex RBD/Nb20 recovery times with each inhibitor, with Boceprevir

Table 4. Results from PLIP docked poses for the RBD/Nb20 interaction with Boceprevir, Calpain Inhibitor II, Calpain Inhibitor XII, and GC376. The index A refers to an amino acid of the Human Nanobody Nb20 receptor and B the ones of the SARS-CoV-2.

Boceprevir					
Hydrophobic Interactions			Hydrogen Bonds		
Amino acid	Residue	Distance [Å]	Amino acid	Residue	Distance H-A [Å]
TYR	117A	3.74	ARG	71A	3.32
TYR	173A	3.64	SER	162B	3.29
TYR	173A	3.97	GLY	164A	2.15
ILE	294B	3.84	ASN	169A	2.58
ILE	294B	3.83	-	-	-
ILE	294B	3.54	-	-	-
Calpain Inhibitor II					
Hydrophobic Interactions			Hydrogen Bonds		
Amino acid	Residue	Distance [Å]	Amino acid	Residue	Distance [Å]
ARG	71A	3.80	GLY	164A	3.20
TYR	163A	3.66	ASN	169A	3.11
PHE	165A	3.64	-	-	-
TYR	173A	3.66	-	-	-
ALA	224B	3.92	-	-	-
GLU	295B	3.75	-	-	-
Calpain Inhibitor XII					
Hydrophobic Interactions			Hydrogen Bonds			π-Stacking		
Amino acid	Residue	Distance [Å]	Amino acid	Residue	Distance H-A [Å]	Amino acid	Residue	Distance [Å]
ARG	71A	3.69	ASN	169A	2.10	HIS	225B	4.55
TYR	163A	3.65	-	-	-	-	-	-
PHE	165A	3.68	-	-	-	-	-	-
TYR	173A	3.68	-	-	-	-	-	-
ILE	294B	3.52	-	-	-	-	-	-
GC376								
Hydrophobic Interactions			Hydrogen Bonds			Salt Bridges		
Amino acid	Residue	Distance [Å]	Amino acid	Residue	Distance H-A [Å]	Amino acid	Residue	Distance [Å]
TYR	173A	3.82	TYR	121A	2.60	ARG	71A	4.98
ILE	294B	3.70	TYR	121A	2.40	-	-	-
GLU	295B	3.99	GLY	164A	3.07	-	-	-
-	-	-	ASN	169A	1.93	-	-	-

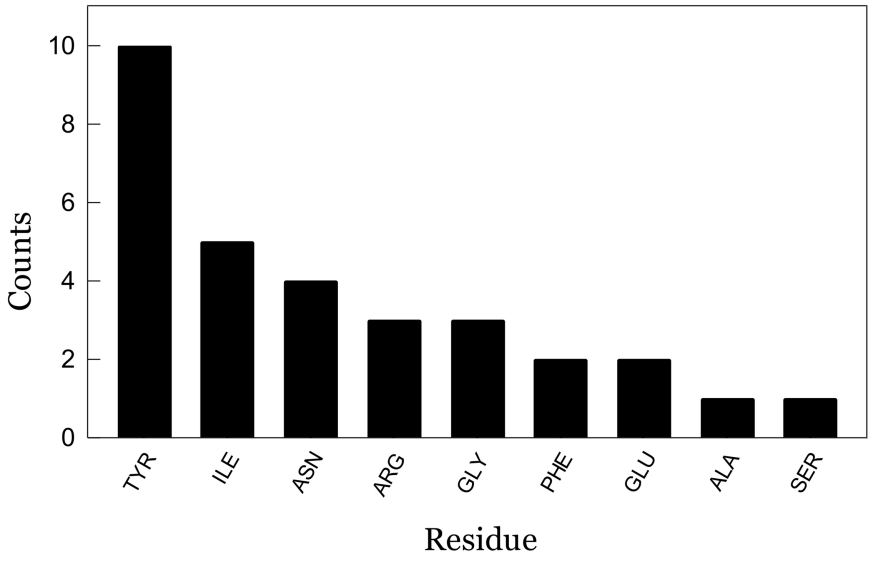

Figure 5. Counts of bonds between ligands and amino acids of a specific kind. This figure suggests that TYR are the crucial amino acid in promoting the attachment to RDB.

Table 5. Recovering time for the complex in the presence of the ligands studied here.

Ligand	τ [s]
Boceprevir	2.08×10^{-7}
Calpain Inhibitor II	8.59×10^{-9}
Calpain Inhibitor XII	3.29×10^{-8}
GC376	2.35×10^{-8}

demonstrating the highest time in order of 10^{-7} s. The recovery time range in order from 10^{-9} s to 10^{-7} s. This order of value indicates that the complex RBD/Nb20 needs a relatively short time to return to what it was before the presence of the inhibitors.

Based on the results of the recovery time, we conducted an MD simulation with a time on the order of the smallest value obtained for the recovery time to investigate whether the ligands can remain unstable or stable at the binding site of the RBD/Nb20 complex within this time frame. This is done using RMSD, the results are illustrated in **Figure 6**. The results show that Boceprevir interacts with the RBD/Nb20 for at least 600 ps, unlinking from the interaction site after this time, as can be seen by the high fluctuations of the RMSD after 600 ps. Calpain Inhibitor II rapidly moves out of the RBD/Nb20 interaction region, which justifies it is having the lowest recovery time value. This can be visualized in the RMSD, which presented high fluctuation in less than 100 ps. The Calpain Inhibitor XII has more time of interaction, with high fluctuation of the RMSD just in about 300 ps, the moment that the ligand moves out for the region of interaction. In about 390 ps, these ligands re-interact with the proteins in one different location, but with high changes of poses along the time, indicating that is not a

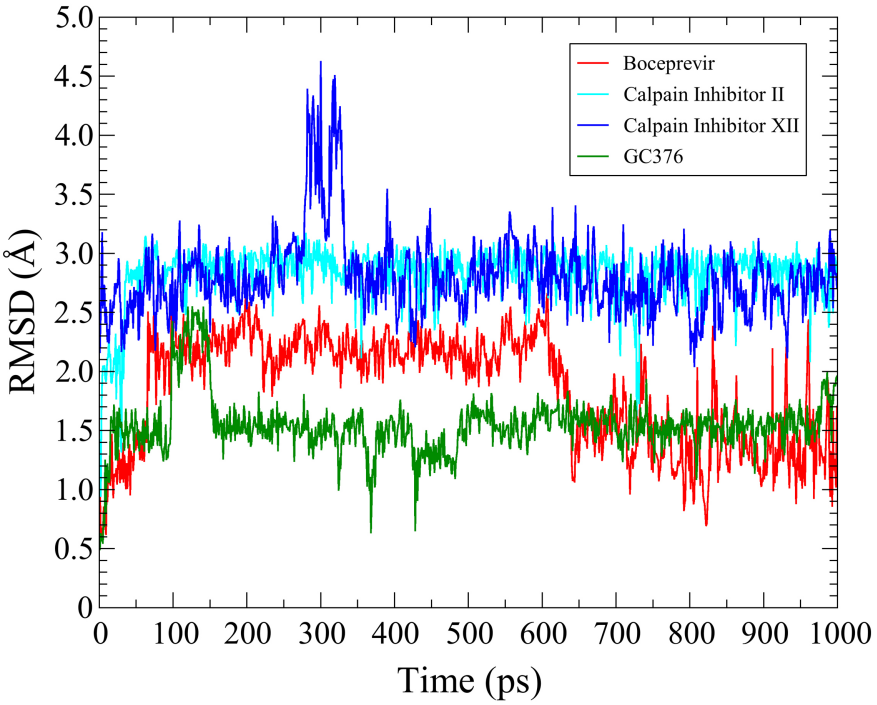

Figure 6. RMSD as a function of the simulation time for the ligands Boceprevir (red line), Calpain Inhibitor II (cyan line), Calpain Inhibitor XII (blue line), and GC376 (green line).

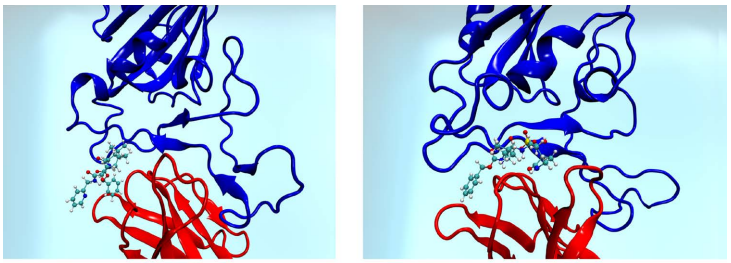

Figure 7. Final pose (at 1000 ps) of RDB/Nb20 proteins with Calpain Inhibitor XII and GC376.

strong interaction. The GC376 presented the more stable interaction, and the RMSD indicates some fluctuations (in about 100 - 200 ps and 360 - 430 ps), but this ligand follows the change in RBD/Nb20 proteins. This trend can be evidenced in the RMSD, which shows little fluctuations over time. The final pose, at 1000 ps, of Calpain Inhibitor XII and GC376 is presented in **Figure 7**.

4. Conclusions

In this study, we used molecular docking and dynamics simulations to examine how Boceprevir, Calpain Inhibitor II, Calpain Inhibitor XII, and GC376 interact with the RBD/Nb20 proteins. Nanobodies, such as Nb20, have shown promise in targeting the RBD of SARS-CoV-2 based on experimental studies. Our analysis of the binding site surface revealed pocket-like regions on the protein complex

that primarily engage in hydrogen bond interactions with the compounds' amino acid residues.

Our findings indicate that the affinity of the interactions ranges from −6.0 Kcal/mol to −7.2 Kcal/mol, with Boceprevir presenting the higher affinity and the Calpain Inhibitor II the minor. Additionally, the recovery time results indicate that the complex RBD/Nb20 can return to what it was before the presence of the inhibitors in a relatively short time, in the order of 10^{-7} s to 10^{-9} s. The MD simulations indicate that Boceprevir exhibits the highest binding affinity but does not fully occupy the binding site, similar to Calpain Inhibitor II. On the other hand, Calpain Inhibitor XII and GC376 interact more extensively with the RBD/Nb20 interface. However, Calpain Inhibitor XII displays high fluctuations and changes in binding poses, whereas GC376 remains stably bound for at least 1000 ps.

Therefore, our results suggest that GC376, in particular, may interfere with the neutralization process of the RBD of SARS-CoV-2 by the human nanobody Nb20. In contrast, the Boceprevir, Calpain Inhibitor II, and Calpain Inhibitor XII can be used simultaneously acting synergistically with the nanobody Nb20 in the process of treatment against SARS-CoV-2.

Acknowledgements

The authors gratefully acknowledge the financial support from Brazilian research agencies CNPq, CAPES, and FAP-DF. L.A.R.J acknowledges the financial support from Brazilian Research Council FAP-DF grants 00193.00001808/2022-71, 00193-00001247/2021-20, 00193-00000857/2021-14, 00193-00001247/2021-20, and 00193-00000811/2021-97 and CNPq grants 302236/2018-0 and 350176/2022-1. This study was financed in part by the Coordenação de Aperfeiçoamento de Pessoal de Nível Superior-Brasil (CAPES)-Finance Code 88887.691997/2022-00. R.G. and L.A.R.J acknowledge CENAPAD-SP for providing computational facilities. L.A.R.J. gratefully acknowledges the support from ABIN grant 08/2019. L.A.R.J. acknowledges Núcleo de Computação de Alto Desempenho (NACAD) for providing the computational facilities through the Lobo Carneiro supercomputer. L.A.R.J. acknowledges the National Laboratory for Scientific Computing (LNCC/MCTI, Brazil) for providing HPC resources of the SDumont supercomputer (URL: http://sdumont.lncc.br), which have contributed to the research results reported within this paper. RTDS is supported by CNPq—Brazilian National Research Council (Grant 310941/2022-9 PQ-1D), FAPDF—Brazilian Federal District Research Support Foundation (Grant 625/2022 SISTεR City), and the University of Brasilia (Grant 7129 UnB COPEI).

Conflicts of Interest

The authors confirm that there is no conflict of interest.

References

[1] Carlos, W.G., Dela Cruz, C.S., Cao, B., Pasnick, S. and Jamil, S. (2020) COVID-19

Disease Due to SARS-CoV-2 (Novel Coronavirus). *American Journal of Respiratory and Critical Care Medicine*, **201**, 7-8. https://doi.org/10.1164/rccm.2014P7

[2] Unal, M. and Irez, T. (2020) COVID 19 Disease Caused by Coronavirus 2 (SARS-CoV-2) (Severe Acute Respiratory Syndrome). *Asian Journal of Medicine and Health*, **18**, 1-11. https://doi.org/10.9734/ajmah/2020/v18i430194

[3] Flor, L.S., Friedman, J., Spencer, C.N., Cagney, J., Arrieta, A., Herbert, M.E., Stein, C., Mullany, E.C., Hon, J., Patwardhan, V., *et al*. (2022) Quantifying the Effects of the COVID-19 Pandemic on Gender Equality on Health, Social, and Economic Indicators: A Comprehensive Review of Data from March, 2020, to September, 2021. *The Lancet*, **399**, 2381-2397. https://doi.org/10.1016/S0140-6736(22)00008-3

[4] Shiels, M.S., Haque, A.T., de Gonz´alez, A.B. and Freedman, N.D. (2022) Leading Causes of Death in the US during the COVID-19 Pandemic, March 2020 to October 2021. *JAMA Internal Medicine*, **182**, 883-886. https://doi.org/10.1001/jamainternmed.2022.2476

[5] Elo, I.T., Luck, A., Stokes, A.C., Hempstead, K., Xie, W.B. and Preston, S.H. (2022) Evaluation of Age Patterns of COVID-19 Mortality by Race and Ethnicity from March 2020 to October 2021 in the US. *JAMA Network Open*, **5**, e2212686. https://doi.org/10.1001/jamanetworkopen.2022.12686

[6] Aria, H., Mahmoodi, F., Ghaheh, H.S., Zare, H., Heiat, M., Bakherad, H., *et al*. (2022) Outlook of Therapeutic and Diagnostic Competency of Nanobodies against SARS-CoV-2: A Systematic Review. *Analytical Biochemistry*, **640**, Article ID: 114546. https://doi.org/10.1016/j.ab.2022.114546

[7] World Health Organization (2021) WHO Coronavirus (COVID-19) Dashboard with Vaccination Data. https://covid19.who.int/

[8] Our World in Data (2023) Coronavirus (COVID-19) Vaccinations. https://ourworldindata.org/covid-vaccinations

[9] Kar, S., Devnath, P., Emran, T.B., Tallei, T.E., Mitra, S. and Dhama, K. (2022) Oral and Intranasal Vaccines against SARS-CoV-2: Current Progress, Prospects, Advantages, and Challenges. *Immunity, Inflammation and Disease*, **10**, e604. https://doi.org/10.1002/iid3.604

[10] Dhama, K., Dhawan, M., Tiwari, R., Emran, T.B., Mitra, S., Rabaan, A.A., Alhumaid, S., Al Alawi, Z. and Al Mutair, A. (2022) COVID-19 Intranasal Vaccines: Current Progress, Advantages, Prospects, and Challenges. *Human Vaccines & Immunotherapeutics*, **18**, e2045853. https://doi.org/10.1080/21645515.2022.2045853

[11] Stander, J., Mbewana, S. and Meyers, A.E. (2022) Plantderived Human Vaccines: Recent Developments. *BioDrugs*, **36**, 573-589. https://doi.org/10.1007/s40259-022-00544-8

[12] Soleymani, S., Tavassoli, A. and Housaindokht, M.R. (2022) An Overview of Progress from Empirical to Rational Design in Modern Vaccine Development, with an Emphasis on Computational Tools and Immunoinformatics Approaches. *Computers in Biology and Medicine*, **140**, Article ID: 105057. https://doi.org/10.1016/j.compbiomed.2021.105057

[13] Cheng, M.H., Krieger, J.M., Banerjee, A., Xiang, Y.F., Kaynak, B., Shi, Y., Arditi, M. and Bahar, I. (2022) Impact of New Variants on SARS-CoV-2 Infectivity and Neutralization: A Molecular Assessment of the Alterations in the Spike-Host Protein Interactions. *iScience*, **25**, Article ID:103939. https://doi.org/10.1016/j.isci.2022.103939

[14] Tang, Q.L., Owens, R.J. and Naismith, J.H. (2021) Structural Biology of Nanobodies against the Spike Protein of SARS-CoV-2. *Viruses*, **13**, Article 2214.

https://doi.org/10.3390/v13112214

[15] Xia, X.H. (2021) Domains and Functions of Spike Protein in SARS-CoV-2 in the Context of Vaccine Design. *Viruses*, **13**, Article 109. https://doi.org/10.3390/v13010109

[16] Tai, W.B., He, L., Zhang, X.J., Pu, J., Voronin, D., Jiang, S.B., Zhou, Y.S. and Du, L. (2020) Characterization of the Receptor-Binding Domain (RBD) of 2019 Novel Coronavirus: Implication for Development of RBD Protein as a Viral Attachment Inhibitor and Vaccine. *Cellular & Molecular Immunology*, **17**, 613-620. https://doi.org/10.1038/s41423-020-0400-4

[17] Xiang, Y.F., Nambulli, S., Xiao, Z.Y., Liu, H., Sang, Z., Duprex, W.P., Schneidman-Duhovny, D., Zhang, C. and Shi, Y. (2020) Versatile and Multivalent Nanobodies Efficiently Neutralize SARS-CoV-2. *Science*, **370**, 1479-1484. https://doi.org/10.1126/science.abe4747

[18] Pymm, P., Adair, A., Chan, L.J., Cooney, J.P., Mordant, F.L., Allison, C.C., Lopez, E., Haycroft, E.R., O'Neill, M.T., Tan, L.L., *et al*. (2021) Nanobody Cocktails Potently Neutralize SARS-CoV-2 D614G N501Y Variant and Protect Mice. *Proceedings of the National Academy of Sciences*, **118**, e2101918118. https://doi.org/10.1073/pnas.2101918118

[19] Pereira Júnior, M.L., Junior, R.T., Nze, G.D., Giozza, W.F. and Júnior, L.A. (2021) Evaluation of Peppermint Leaf Flavonoids as SARS-CoV-2 Spike Receptor-Binding Domain Attachment Inhibitors to the Human ACE2 Receptor: A Molecular Docking Study. *Open Journal of Biophysics*, **12**, 132-152. https://doi.org/10.4236/ojbiphy.2022.122005

[20] Xiu, S.Y., Dick, A., Ju, H., Mirzaie, S., Abdi, F., Cocklin, S., Zhan, P. and Liu, X.Y. (2020) Inhibitors of SARS-CoV-2 Entry: Current and Future Opportunities. *Journal of Medicinal Chemistry*, **63**, 12256-12274. https://doi.org/10.1021/acs.jmedchem.0c00502

[21] Rodriguez, C., Luque, N., Blanco, I., Sebastian, L., Barber`a, J.A., Peinado, V.I. and Tura-Ceide, O. (2021) Pulmonary Endothelial Dysfunction and Thrombotic Complications in Patients with COVID-19. *American Journal of Respiratory Cell and Molecular Biology*, **64**, 407-415. https://doi.org/10.1165/rcmb.2020-0359PS

[22] Astuti, I., *et al*. (2020) Severe Acute Respiratory Syndrome Coronavirus 2 (SARS-CoV-2): An Overview of Viral Structure and Host Response. *Diabetes & Metabolic Syndrome*: *Clinical Research & Reviews*, **14**, 407-412. https://doi.org/10.1016/j.dsx.2020.04.020

[23] Ma, C.L., Sacco, M.D., Hurst, B., Townsend, J.A. Hu, Y.M., Szeto, T., Zhang, X.J., Tarbet, B., Thomas Marty, M., Chen, Y., *et al*. (2020) Boceprevir, GC-376, and Calpain Inhibitors II, XII Inhibit SARS-CoV-2 Viral Replication by Targeting the Viral Main Protease. *Cell Research*, **30**, 678-692. https://doi.org/10.1038/s41422-020-0356-z

[24] Fu, L.F., Ye, F., Feng, Y., Yu, F., Wang, Q.S., Wu, Y., Zhao, C., Sun, H., Huang, B.Y., Niu, P.H., *et al*. (2020) Both Boceprevir and GC376 Efficaciously Inhibit SARS-CoV-2 by Targeting Its Main Protease. *Nature Communications*, **11**, Article No. 4417. https://doi.org/10.1038/s41467-020-18233-x

[25] Kim, S., Chen, J., Cheng, T.J., Gindulyte, A., He, J., He, S.Q., Li, Q.L., Shoemaker, B.A., Thiessen, P.A., Yu, B., *et al*. (2023) Pubchem 2023 Update. *Nucleic Acids Research*, **51**, D1373-D1380. https://doi.org/10.1093/nar/gkac956

[26] Kochnev, Y., Hellemann, E., Cassidy, K.C. and Durrant, J.D. (2020) Webina: An Open-Source Library and Web App That Runs AutoDock Vina Entirely in the Web

Browser. *Bioinformatics*, **36**, 4513-4515.
https://doi.org/10.1093/bioinformatics/btaa579

[27] Brooks, B.R., *et al*. (2009) CHARMM: The Biomolecular Simulation Program. *Journal of Computational Chemistry*, **30**, 1545-1614. https://doi.org/10.1002/jcc.21287

[28] Salentin, S., Schreiber, S., Haupt, V.J., Adasme, M.F. and Schroeder, M. (2015) Plip: Fully Automated Protein—Ligand Interaction Profiler. *Nucleic Acids Research*, **43**, W443-W447. https://doi.org/10.1093/nar/gkv315

[29] Zhang, X.X., Chen, Z.W., Chen, D.C., Cui, H. and Tang, J. (2020) Adsorption Behaviour of SO_2 and SOF_2 Gas on RH-Doped BNNT: A DFT Study. *Molecular Physics*, **118**, e1580394. https://doi.org/10.1080/00268976.2019.1580394

[30] Timsorn, K. and Wongchoosuk, C. (2020) Adsorption of NO_2, HCN, HCHO and CO on Pristine and Amine Functionalized Boron Nitride Nanotubes by Self-Consistent Charge Density Functional Tight-Binding Method. *Materials Research Express*, **7**, Article ID: 055005. https://doi.org/10.1088/2053-1591/ab8b8b

[31] Peng, S., Cho, K., Qi, P.F. and Dai, H.J. (2004) Ab Initio Study of CNT NO_2 Gas Sensor. *Chemical Physics Letters*, **387**, 271-276.
https://doi.org/10.1016/j.cplett.2004.02.026

[32] Phillips, J.C., Zheng, G.B., Kumar, S. and Kale, L.V. (2002) NAMD: Biomolecular Simulation on Thousands of Processors. *Proceedings of the* 2002 *ACM/IEEE Conference on Supercomputing*, Baltimore, 16-22 November 2002, 36.
https://doi.org/10.1109/SC.2002.10019

[33] Klauda, J.B., Venable, R.M., Freites, J.A., O'Connor, J.W., Tobias, D.J., Mondragon-Ramirez, C., Vorobyov, I., MacKerell Jr, A.D. and Pastor, R.W. (2010) Update of the CHARMM All-Atom Additive Force Field for Lipids: Validation on Six Lipid Types. *The Journal of Physical Chemistry B*, **114**, 7830-7843.
https://doi.org/10.1021/jp101759q

[34] Humphrey, W., Dalke, A. and Schulten, K. (1996) VMD: Visual Molecular Dynamics. *Journal of Molecular Graphics*, **14**, 33-38.
https://doi.org/10.1016/0263-7855(96)00018-5

[35] Fukunishi, Y., Yamashita, Y., Mashimo, T. and Nakamura, H. (2018) Prediction of Protein-Compound Binding Energies from Known Activity Data: Docking-Score-Based Method and Its Applications. *Molecular Informatics*, **37**, Article ID: 1700120.
https://doi.org/10.1002/minf.201700120

[36] Guler, H.I., Tatar, G., Yildiz, O., Belduz, A.O. and Kolayli, S. (2021) Investigation of Potential Inhibitor Properties of Ethanolic Propolis Extracts against ACE-II Receptors for COVID-19 Treatment by Molecular Docking Study. *Archives of Microbiology*, **203**, 3557-3564. https://doi.org/10.1007/s00203-021-02351-1

[37] Khayrani, A.C., Irdiani, R., Aditama, R., Pratami, D.K., Lischer, K., Ansari, M.J., Chinnathambi, A., Ali Alharbi, S., Almoallim, H.S. and Sahlan, M. (2021) Evaluating the Potency of Sulawesi Propolis Compounds as ACE-2 Inhibitors through Molecular Docking for COVID-19 Drug Discovery Preliminary Study. *Journal of King Saud University-Science*, **33**, Article ID: 101297.
https://doi.org/10.1016/j.jksus.2020.101297

[38] Towler, P., Staker, B., Prasad, S.G., Menon, S., Tang, J., Parsons, T., Ryan, D., Fisher, M., Williams, D., Dales, N.A., *et al*. (2004) ACE2 X-Ray Structures Reveal a Large Hinge-Bending Motion Important for Inhibitor Binding and Catalysis. *Journal of Biological Chemistry*, **279**, 17996-18007.
https://doi.org/10.1074/jbc.M311191200